

Polymer Chemistry

Accepted Manuscript



This is an *Accepted Manuscript*, which has been through the Royal Society of Chemistry peer review process and has been accepted for publication.

Accepted Manuscripts are published online shortly after acceptance, before technical editing, formatting and proof reading. Using this free service, authors can make their results available to the community, in citable form, before we publish the edited article. We will replace this *Accepted Manuscript* with the edited and formatted *Advance Article* as soon as it is available.

You can find more information about *Accepted Manuscripts* in the [Information for Authors](#).

Please note that technical editing may introduce minor changes to the text and/or graphics, which may alter content. The journal's standard [Terms & Conditions](#) and the [Ethical guidelines](#) still apply. In no event shall the Royal Society of Chemistry be held responsible for any errors or omissions in this *Accepted Manuscript* or any consequences arising from the use of any information it contains.

Cite this: DOI: 10.1039/coxx00000x

www.rsc.org/xxxxxx

ARTICLE TYPE

Tiny nanoparticles of organometallic polymers through direct disassembly-assisted synthesis strategy for hydrogen peroxide sensing†

Guodong Liang,^{*a} Xiaodong Li,^a Bin Fei,^{*b} Xiaomei Wang^a and Fangming Zhu^a*Received (in XXX, XXX) Xth XXXXXXXXXX 20XX, Accepted Xth XXXXXXXXXX 20XX*

DOI: 10.1039/b000000x

Hybrid nanostructures present a catalog of promising functional materials with a broad range of applications. Structural control has been proved versatile to optimize functions and properties of the nanomaterials. Although polymer/inorganic hybrid nanoparticles have been achieved through self-assembly of block copolymers, synthesis of hybrid nanoparticles with small size (≤ 20 nm) remains challenging. Herein, we developed a conceptually new approach for efficient and scalable synthesis of polymer/inorganic hybrid nanoparticles with well-defined shape and tiny size through direct disassembly-assisted synthesis (DDAS) strategy. Incorporating cyanoferrate into polypeptides led to disassembly of large hexagonally-packed structures of polypeptide α -helices into small aggregates. Subsequent coordination polymerization of the cyanoferrate groups with Fe^{3+} in aqueous media afforded polypeptide/Prussian blue (PB) hybrid nanoparticles with well-defined core-shell structures. Hybrid nanoparticles were thoroughly characterized. Morphological and microstructural analyses showed that the hybrid nanoparticles had small size of approximately 18 nm and crystalline PB phase. Taking advantage of tiny size and crystalline PB phase, the hybrid nanoparticles showed excellent electrocatalytic activity toward reduction of hydrogen peroxide. Such direct disassembly-assisted synthesis of polymer/inorganic tiny nanoparticles provides a family of functional nanomaterials useful for biosensing and nanodevice applications.

Introduction

Polymer/inorganic hybrid nanostructures present a catalog of promising functional nanomaterials where polymer and inorganic constituents are compounded at molecule level with at least one dimension at nanoscale.^{1, 2} Due to large surface and multiple components, hybrid nanomaterials exhibit exceptional mechanical, magnetic, and conductive properties.³ Compared with inorganic nanoparticles, hybrid nanostructures exhibit superior stability and solubility, excellent biocompatibility, low cytotoxicity, and superb flexibility with a broad range of applications in biological, clean energy, and optical device fields.⁴ The functions and properties of hybrid nanostructures can be optimized by tuning their size and morphology as well as constituents, strongly depending on synthetic protocols applied. Developing new synthetic strategy to synthesize hybrid nanomaterials is extremely important for exploiting new nanomaterials with high performances and novel functions.

To date, a number of techniques including supercritical fluid,⁵ microfluidic,⁶ and self-assembly have been developed to synthesize polymer/inorganic hybrid nanomaterials. Among them, self-assembly of block copolymers has received particular interests due to tuneable morphology and size, ease of fabrication, and mass production of nanoparticles.⁷⁻¹⁸ Block copolymers self

assemble into regular nanoaggregates in solution, which are used as templates to grow *in situ* inorganic nanoparticles on it. This affords polymer/inorganic hybrid nanoparticles with controlled morphology and size. MacLachlan and coworkers synthesized polymer/Prussian blue (PB) nanocapsules through combining self-assembly of an amphiphilic block copolymer containing cyanoferrate groups with subsequent coordination polymerization of the cyanoferrate groups.^{19, 20} Polymer/PB nanoshells were achieved by using miniemulsion periphery polymerization (MEPP).²¹ In addition, hybrid nanoparticles with various morphologies including nanosphere, nanocubes, and nanowire coils have also been synthesized based on block copolymer templates.²²⁻²⁹ An alternative approach to hybrid nanomaterials is using block copolymers to direct arrangement of inorganic particles. Self-assembly of copolymers in bulks induces inorganic particles to align in a controlled manner, affording hybrid nanomaterials with well-defined architectures.³⁰⁻³² Liu and coworkers synthesized polymer/gold hybrid micelles, vesicles, and rods through self-assembly of gold nanoparticles tethered to amphiphilic block copolymers.³³ Polymer/gold capsules and spheres were achieved by means of direct assembly of gold-containing block copolymers.^{34, 35}

Recently, tiny nanoparticles with small size have received particular interests, because the surface area of nanoparticles

increases drastically with decreasing particle size. In small nanoparticles with large surface area, most of the atoms are exposed to the surface. Such active atoms endow nanoparticles unpredictable properties. For instance, tiny carbon nanoparticles (or carbon dots) and gold nanodots emit intense fluorescence,^{36,37} which are not observed in their bulks. Moreover, polymer chains on the surface exhibit quite different dynamic behaviour as in bulks.^{38,39} The surface effect is more significant for smaller particles. Fundamentally understanding the size effect of dynamics of polymers in nanoparticles is still in lack.³⁹ On the other hand, Trends of device miniaturation also require exploring functional nanoparticles with tiny size.

The size of nanoparticles self-assembled through block copolymers depends on constituent and molecular weight of copolymers. Chain length of polymers is in the range of a few nanometers to tens of nanometers. Tens of thousands of copolymer chains gather together to form nanoparticles with size ranging from 40 nm to a few hundred nanometers. Although decreasing molecular weight of polymers results in small particles to some extent, it is difficult to synthesize nanoparticles smaller than 20 nm, because low molecular weight of copolymers inevitably leads to decreased phase-separation strength, which is driving force for the formation of nanoparticles. Decreased phase-separation strength subsequently results in ill-defined nanoparticles. Consequently, it seems that it is unwise to fabricate tiny nanoparticles through self-assembly of block copolymers. Keep polymers having a chain length of a few nanometers in mind, it is favorable to take an opposite strategy, disassembly rather than self-assembly of polymers, namely “splitting” a few polymer chains from large aggregates to form tiny aggregates or nanoparticles.

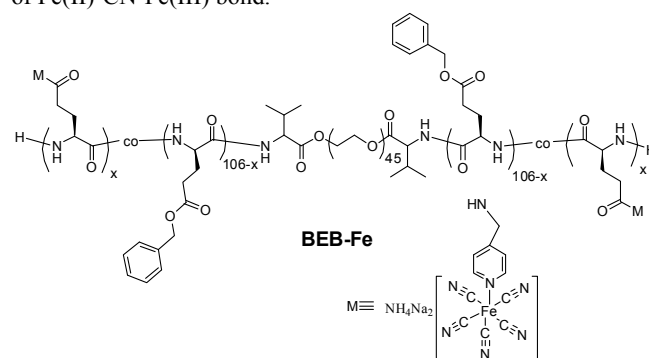
Recently, Aida and coworkers manipulated discrete nanorings through disassembly of self-assembled nanotubes of ferrocene motif and AgBF_4 .⁴⁰ Janus nanodiscs were also synthesized using stepwise disassembly of self-assembled aggregates of PS-*b*-P4VP block copolymer (PS: polystyrene; P4VP: poly(4-vinylpyridine)).⁴¹ Although such assembly-disassembly strategy allows for the synthesis of tiny nanoparticles, they suffered from some inherent limits including complicated procedures, rigorous conditions, and broad size distribution. Therefore, developing new strategies for the synthesis of tiny nanoparticles is highly desirable. Previously, we synthesized poly(γ -benzyl-L-glutamate) (PBLG) decorated with cyanoferrate groups. We found that grafting cyanoferrate groups to the sidechain of PBLG destroyed the packing structure of PBLG α -helices.⁴²⁻⁴⁴ Inspired by this finding, herein, we developed a conceptually new approach for scalable synthesis of polymer/inorganic hybrid nanoparticles with well-defined microstructures and tiny size through direct disassembly-assisted synthesis (DDAS) strategy. Incorporating cyanoferrate into polypeptides led to disassembly of large hexagonally-packed structures of polypeptide α -helices into small aggregates. Subsequent coordination polymerization of the cyanoferrate groups with Fe^{3+} in aqueous media afforded polypeptide/Prussian blue (PB) hybrid nanoparticles with well-defined core-shell structures. The hybrid nanoparticles had small size of approximately 18 nm and crystalline PB phase. Taking advantage of tiny size and crystalline PB phase, the hybrid nanoparticles showed excellent electrocatalytic activity toward

reduction of hydrogen peroxide. Compared with assembly-disassembly strategy, the advantages of DDAS are straightforward: (1) direct disassembly of naturally-occurring polypeptide structures, evading the susceptible assembly process; (2) simple and easy synthetic procedure. With these merits, direct disassembly-assisted synthesis of polymer/inorganic tiny nanoparticles provides a family of functional nanomaterials useful for biosensing and nanodevice applications.

Results and discussion

Synthesis of BEB-PB nanoparticles

Poly(γ -benzyl-L-glutamate)-*b*-poly(ethylene glycol)-*b*-poly(γ -benzyl-L-glutamate) triblock copolymers selectively decorated with cyanoferrate complex (BEB-Fe, Scheme 1) have been previously synthesized in our lab.⁴² In this work, BEB-Fe was used as a precursor to synthesize polymer/inorganic hybrid nanoparticles. BEB-Fe was dissolved in distilled water to get a transparent yellow solution. Upon the addition of Fe^{3+} , the yellow solution changed into dark blue immediately. UV-vis spectra (Fig. 1) showed that a distinct absorbance at 718 nm appeared upon the addition of Fe^{3+} , ascribed to charge transfer of Fe(II)-CN-Fe(III) .^{45,46} This revealed that cyanoferrate groups of BEB-Fe coordinated with Fe^{3+} . Moreover, the absorbance at 718 nm increased linearly with increasing the amount of Fe^{3+} until one equivalent mole of Fe^{3+} was added, which indicated that Fe^{3+} involved in the coordination reaction. In FT-IR spectra, a strong absorbance band at 2060 cm^{-1} was observed for BEB-Fe, attributed to stretching vibration of $\text{C}\equiv\text{N}$. This band shifted to 2080 cm^{-1} after coordination polymerization due to the formation of Fe(II)-CN-Fe(III) bond.^{47,48}



Scheme 1 Chemical structure of poly(γ -benzyl-L-glutamate)-*b*-poly(ethylene glycol)-*b*-poly(γ -benzyl-L-glutamate) triblock copolymer modified with cyanoferrate complex (BEB-Fe).

Moreover, absorbance bands at 1655 cm^{-1} and 1545 cm^{-1} , characteristic of α -helix conformation of PBLG, were observed for BEB, BEB-Fe, and BEB-PB (Fig. 2).⁴⁹ This demonstrated that PBLG adopted α -helix conformation in BEB, BEB-Fe, and BEB-PB, independent of the incorporation of cyanoferrate and the formation of PB. The possible reason is that cyanoferrate groups pending along PBLG chains are located at the outside of PBLG helices due to electrostatic repulsion interaction, which takes an

insignificant effect on the confirmation of PBLG backbone.

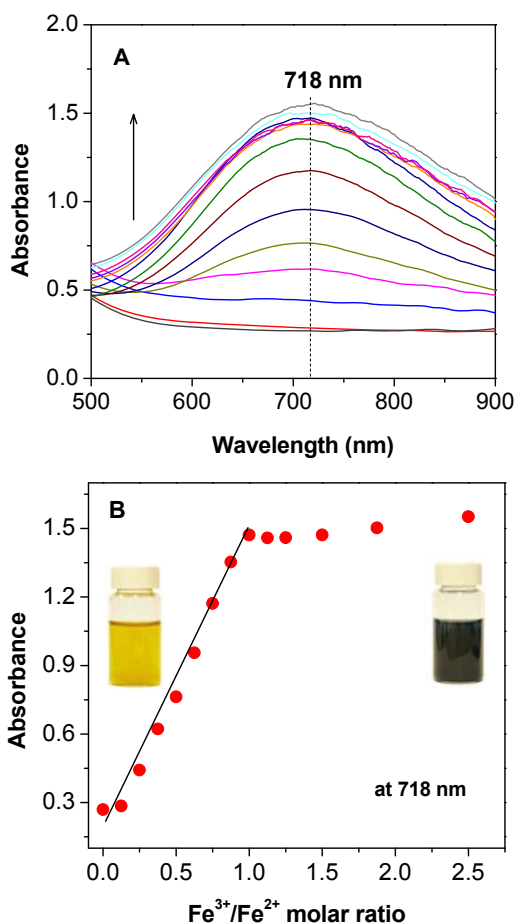


Fig. 1 (A) UV-vis spectra of BEB-Fe with various amounts of Fe³⁺ and (B) variation of absorbance at 718 nm against the mole ratio of Fe³⁺ to ferrate complex. Inset showed digital photos of BEB-Fe before (left) and after (right) addition of Fe³⁺. The concentration of BEB-Fe was 0.25 mg/mL.

Chain conformation of PBLG in BEB-PB was further investigated using circular dichroism spectrometry (CD), as shown in Fig. 3. Two negative signals at 208 nm and 222 nm, attributed to $\pi \rightarrow \pi^*$ and $n \rightarrow \pi^*$ transition of PBLG α -helices, respectively, were observed for BEB-PB, showing that PBLG existed as α -helix in BEB-PB.⁵⁰ This verified that incorporation of cyanoferrate and the formation of PB did not destroy noticeably α -helix conformation of PBLG backbone, consistent with FT-IR results.

20 Morphology and microstructure of BEB-PB nanoparticles

Previously, we demonstrated that incorporation of a proper amount of cyanoferrate complex into PBLG could destroy hexagonally-packed structure of PBLG α -helices.⁴² Thus, it is interesting to investigate the effect of cyanoferrate fraction on the size of BEB-PB particles. Particle size of BEB-PB was monitored using dynamic light scattering (DLS). For the purpose of comparison, the size of BEB was also measured. The hydrodynamic diameter of BEB suspended in aqueous media was

approximately 160 nm with broad size distribution, as shown in Fig. 4 and Table 1. Small size of 94 nm was obtained for BEB-PB5 (using BEB-Fe5 as precursor which contained 4.7 wt% cyanoferrate). Further increasing cyanoferrate fraction led to gradually decreasing of the size of BEB-PB nanoparticles. When cyanoferrate fraction reached 25.6 wt%, particle size decreased to 20 nm (BEB-PB26). The incorporation of cyanoferrate destroys the stacking structure of PBLG α -helices. BEB-Fe suspended in aqueous media formed micelles with cyanoferrate residing in the periphery. Upon addition of Fe³⁺, cyanoferrate in periphery coordinated with Fe³⁺ to form polymer/Prussian blue (BEB-PB) nanoparticles, as shown in Scheme 2.

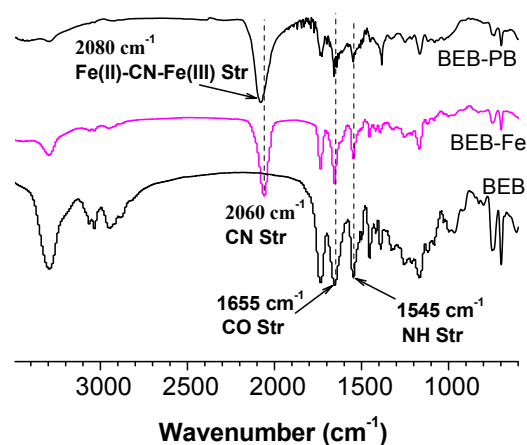


Fig. 2 FT-IR spectra of BEB, BEB-Fe, and BEB-PB nanoparticles.

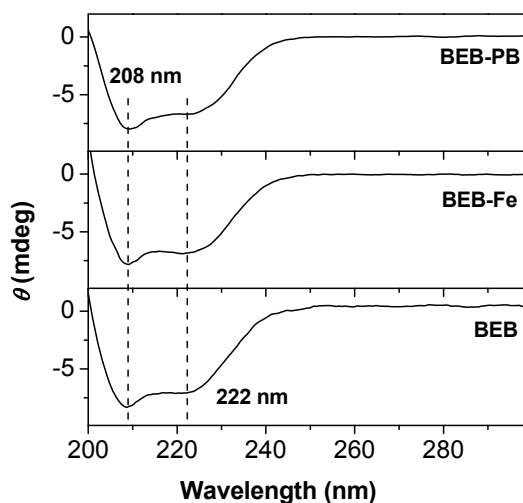


Fig. 3 Circular dichroism (CD) spectra of BEB, BEB-Fe, and BEB-PB dissolved/suspended in acetonitrile.

The morphology of BEB-PB suspended in aqueous media was observed using transmission electron microscopy (TEM) and atomic force microscopy (AFM), as shown in Fig. 5. Spherical particles with a size of approximately 140 nm were observed in TEM images of BEB. While uniform particles with a size of 18 nm were observed for BEB-PB26. TEM image at higher magnitudes revealed that BEB-PB tiny nanoparticles had a core-

shell structure. AFM image further verified spherical nanoparticles of BEB-PB (Fig. 5F). The particle size determined by TEM agreed well with the results by DLS. The length of PBLG α -helices was estimated to be $106/3.6 \times 0.54 \text{ nm} = 15.9 \text{ nm}$ (where 106 was the number of repeating units of PBLG) by considering 18/5 α -helical conformation to have a length of 0.54 nm for each pitch of the helix.⁵¹ The size of BEB-PB26 nanoparticles (18 nm) was close to the length of PBLG α -helices (15.9 nm).

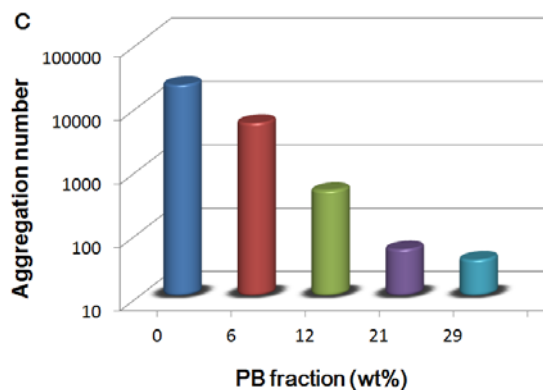
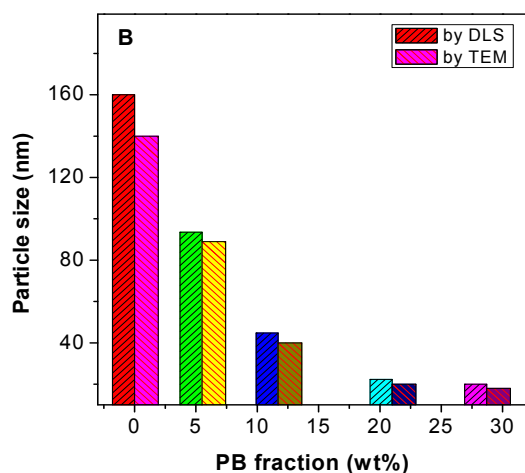
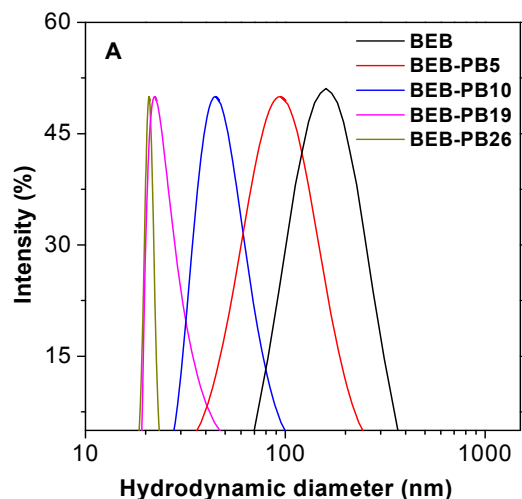


Fig. 4 (A) DLS curves, (B) particle size and (C) aggregation number of BEB-PB nanoparticles with various PB fractions.

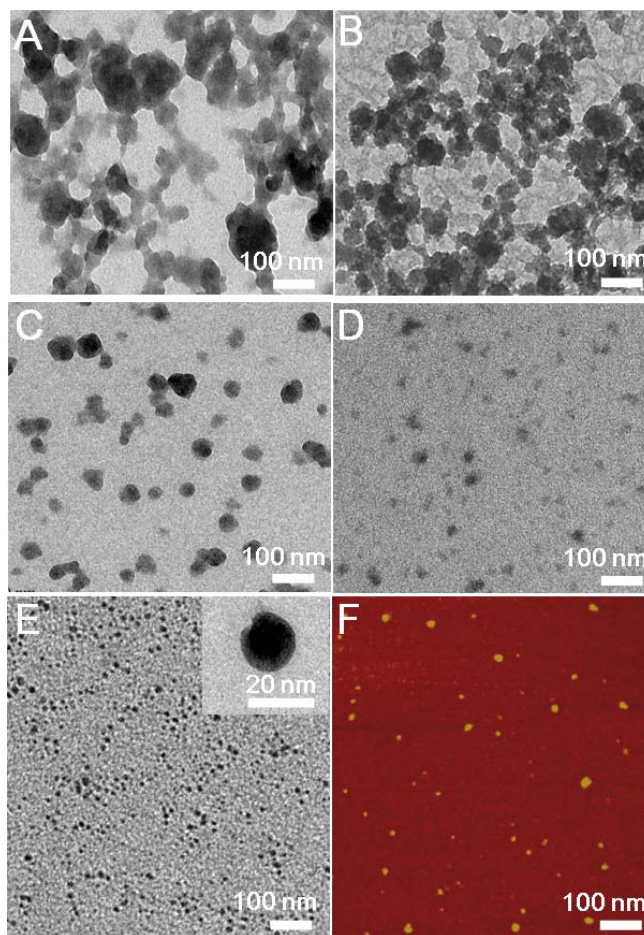


Fig. 5 TEM images of BEB-PB with various PB fractions (A-E: BEB, BEB-PB5, BEB-PB10, BEB-PB19, BEB-PB26, respectively) and height image of tapping mode AFM image of BEB-PB26 (F). Inset of image E was a TEM image at high magnitudes of BEB-PB26.

Aggregation number of BEB and BEB-PB nanoparticles was estimated based on particle size by TEM (Fig. 4, Table 1 and see Electronic Supplementary Information (ESI)). BEB aggregates have a huge aggregation number of 21000. The aggregation number of BEB-PB nanoparticles decreased drastically with increasing cyanoferrate fractions of BEB-Fe. BEB-PB26 had an aggregation number as small as 37, three orders of magnitude lower than that of BEB. Possible reason is that with increasing cyanoferrate fractions of BEB-Fe, large hexagonally-packed structures of PBLG α -helices disassemble into small pieces due to electrostatic repulsion interaction among negatively-charged cyanoferrate groups. This leads to a decreased aggregation number of BEB-PB with high PB fractions.

The microstructure of BEB-PB nanoparticles was investigated using X-ray diffractometry (XRD) (Fig. 6). BEB showed a diffraction peak at 6.43° , ascribed to hexagonally-stacked α -helices of PBLG (Scheme 2). The distance between adjacent α -helices of PBLG was determined to be 1.58 nm.⁴² The diffraction peak disappeared for BEB-Fe26, indicating that the hexagonally-stacked structure of PBLG was destroyed in BEB-Fe. Similarly, no hexagonally-stacked structures of PBLG α -helices

were detected in BEB-PB26, possibly due to random-arranged PBLG α -helices and small aggregation number of BEB-PB26. Moreover, two diffraction peaks at 17.5 ° and 24.6 °, attributed to the (200) and (220) indices of cubic PB crystals (JCPDS card No

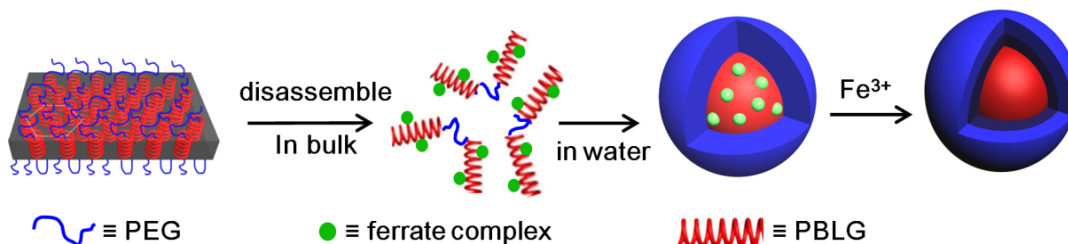
5 73-0687), were observed for BEB-PB26, revealing the formation of crystalline PB phase in BEB-PB26 possibly due to high cyanoferrate fractions of BEB-Fe26.

Table 1 Particle size, aggregation number, and electrochemical parameters of BEB-PB nanoparticles.

BEB-PB	BEB-Fe	^a W_c (wt%)	^b W_{PB} (wt%)	^c D_h (nm)	^d D (nm)	^e Aggreg. number	$E_p^{1/2}$ (V)	ΔE_p (V)	i_{pa} (μA)
BEB	BEB	0	0	160	140	21000	/	/	/
BEB-PB5	BEB-Fe5	4.7	5.5	94	89	5300	0.189	0.165	0.2
BEB- PB10	BEB-Fe10	10.2	11.7	45	40	460	0.183	0.124	1.5
BEB- PB19	BEB-Fe19	18.5	21.0	22	20	54	0.183	0.112	14.5
BEB- PB26	BEB-Fe26	25.6	28.7	20	18	37	0.180	0.060	23.4

^a W_c denoted weight fractions of ferrate complex in BEB-Fe. ^b W_{PB} denoted weight fraction of Prussian blue in BEB-PB, calculated by using $W_{PB} = W_c(M_c + M_{Fe}) / (M_c + M_{Fe} \cdot W_c)$ where M_c and M_{Fe} were molecular weight of ferrate complex and iron, respectively. ^c D_h was determined by DLS, ^d D was determined by TEM. ^eCalculation of aggregation number (N) was shown in Electronic Supplementary Information (ESI).

15



Scheme 2 Schematic illustration of direct disassembly-assisted synthesis of tiny polymer nanoparticles.

20

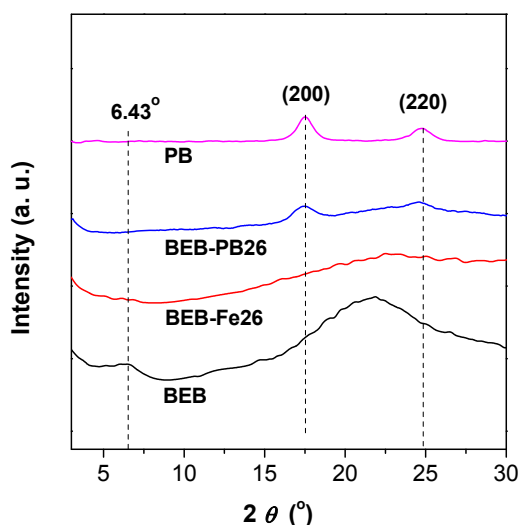


Fig. 6 XRD curves of BEB, BEB-Fe, BEB-PB, and conventional PB particles.

25 Electrochemical performance of BEB-PB nanoparticles

Given crystalline PB phase and tiny size of BEB-PB hybrid

nanoparticles, it is interesting to investigate the electrochemical performance of BEB-PB nanoparticles using cyclic voltammogram (CV). Typical CV curves of BEB-PB nanoparticles showed a redox pair at $E_p^{1/2} = 0.18$ V, attributed to reversible Prussian white/Prussian blue conversion.⁵² Interestingly, the peak current of BEB-PB nanoparticles increased, while peak separation decreased with increasing PB fractions (Fig. 7 and Table 1). PB is electrochemically active. Increasing PB fractions leads to enhanced redox current and decreased peak separation of BEB-PB nanoparticles. Moreover, with increasing PB fractions, size of BEB-PB nanoparticles drops sharply, which favors electrical contact between PB and electrode due to the enhanced surface area of BEB-PB tiny nanoparticles.

40 Encouraged by the large redox current of tiny nanoparticles of BEB-PB26, we investigated the electrocatalytic activity of BEB-PB26 toward reduction of hydrogen peroxide (H_2O_2) (Fig. 8). The electrochemical reduction of H_2O_2 started on 0.31 V, positively shifted by 0.10 V compared with the bare glassy carbon electrode (Fig. S1, ESI). It is noted that the onset potential was close to that of reduction of Prussian blue to Prussian white. This demonstrated that BEB-PB26 tiny nanoparticles served as electron mediator for the reduction of H_2O_2 . Maximum reduction current plateau of 79 μA was obtained at low potentials (< 0 V), 50 20-fold of that for conventional PB particles (Fig. S2, ESI) under identical measurement conditions. The significantly improved

reduction current possibly derives from tiny size of BEB-PB26 nanoparticles with large surface area, which favours efficient contact among PB, H₂O₂ molecules, and electrodes.

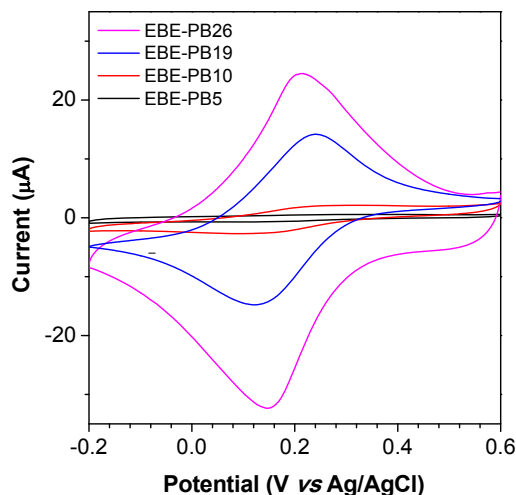


Fig. 7 Cyclic voltammogram of BEB-PB nanoparticles deposited on glassy carbon electrodes, 20 mM sodium phosphate buffer solution, scan rate 50 mV s⁻¹, under N₂.

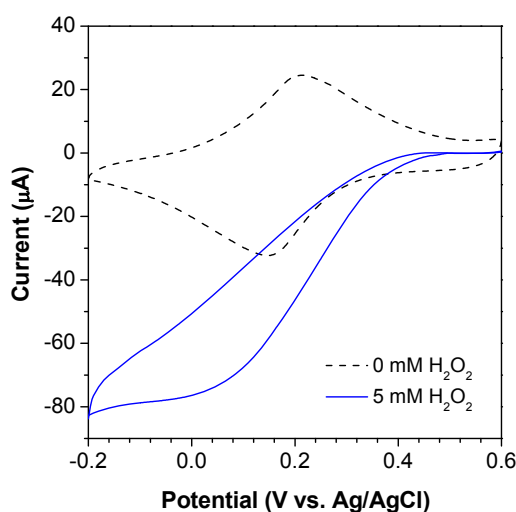


Fig. 8 Cyclic voltammogram of BEB-PB26 tiny nanoparticles deposited on glassy carbon electrodes in the presence of 5 mM H₂O₂ (solid curve). 20 mM sodium phosphate buffer solution, scan rate 50 mV s⁻¹, under N₂.

We further investigated current trace of BEB-PB26 tiny nanoparticles upon stepwise addition of H₂O₂ (Fig. 9). For the purpose of comparison, current traces of bare electrode and conventional PB particles were also conducted. Conventional PB particles with irregular morphology and size of approximately 300 nm showed small current response to H₂O₂. 5-fold enhancement of current response was observed for BEB-PB26 tiny nanoparticles. The detection limit was determined to be 18 nM, comparable to that for PB nanostructures in literatures.^{53, 54}

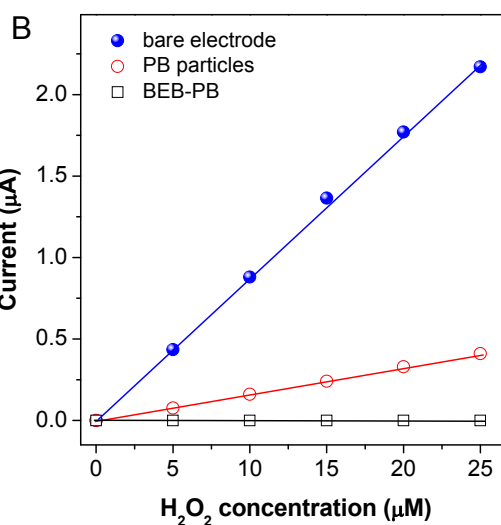
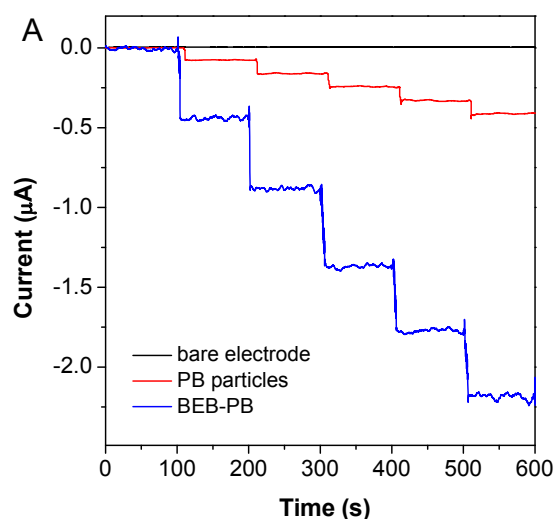


Fig. 9 (A) Current traces of EBE-PB26 deposited on glassy carbon electrode upon stepwise addition of H₂O₂ (5 µM each step) and (B) plots of current against H₂O₂ concentration. Sodium phosphate buffer solution (20 mM), pH: 7.4, under N₂. Applied potential: 0.1 V.

Finally, we evaluated successive performance ability of sensor based on BEB-PB26 tiny nanoparticles. The cathodic currents for reduction of H₂O₂ as a function of time for BEB-PB nanoparticles and conventional PB particles were shown in Fig. 10. The cathodic current of conventional PB particles dropped drastically with time, and lost 40% of their initial current after 2 h. In contrast, BEB-PB26 tiny nanoparticles retained 86% of their initial current after 2 h. This revealed that BEB-PB26 tiny nanoparticles possessed improved operational stability contrasting to conventional PB particles. Possible reason is that electrochemically active PB layers are tethered to electrochemically inert PBLG segments, which prevents the labile Prussian white reduced during electrochemical reduction of Prussian blue from leaking.^{55, 56}

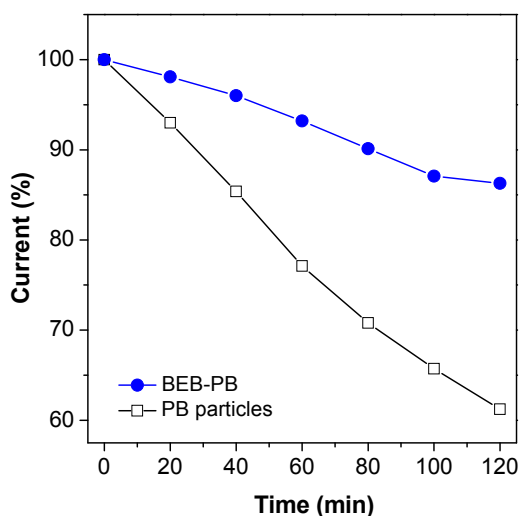


Fig. 10 Successive performance ability of BEB-PB26 tiny nanoparticles deposited on glassy carbon electrode in 20 mM sodium phosphate buffer solution in the presence of 5 mM H₂O₂. Applied potential: 0.1 V, under N₂.

Conclusions

In summary, we developed a conceptually new approach for scalable synthesis of polymer/inorganic hybrid nanoparticles with well-defined shapes and tiny size through direct disassembly-assisted synthesis (DDAS) strategy. Incorporating cyanoferrate into polypeptides led to disassembly of large hexagonally-packed structures of polypeptide α -helices into small aggregates. Subsequent coordination polymerization of the cyanoferrate groups with Fe³⁺ in aqueous media afforded polypeptide/Prussian blue (PB) hybrid nanoparticles with well-defined core-shell structures. The hybrid nanoparticles had small size of approximately 18 nm and PB crystalline phase. Taking advantage of tiny size and PB crystalline phase, the hybrid nanoparticles showed excellent electrocatalytic activity toward reduction of hydrogen peroxide. Moreover, sensors based on the hybrid nanoparticles showed by far higher operation stability contrasting to conventional PB particles. Such polymer/inorganic tiny nanoparticles by DDAS provide a class of functional nanomaterials with applications in biosensing and nanodevices.

Experimental

Materials

Poly(γ -benzyl-L-glutamate)-*b*-poly(ethylene glycol)-*b*-poly(γ -benzyl-L-glutamate) triblock copolymers selectively decorated with cyanoferrate complex (BEB-Fe) were synthesized previously in our lab.⁴² Chemical structure and parameters of BEB-Fe used were shown in Scheme 1 and Table 1. Fe(NO₃)₃·9H₂O, methanol, acetonitrile, and sodium phosphate were purchased from Sigma-Adrich (China) and used without further purification unless otherwise indicated.

Synthesis

To synthesize polymer/Prussian blue (PB) hybrid nanoparticles, 50 mg of BEB-Fe was suspended in 10 mL of distilled water with the assistance of sonication. To the BEB-Fe suspension was added 2 equivalent moles of Fe(NO₃)₃ aqueous solution. The mixture was stirred for 12 h at room temperature. The resulting solution was added dropwise into 100 mL of cold methanol with stirring. The mixture was centrifuged and the top layer was decanted. The solid was rinsed with cold methanol (50 mL \times 3) and dried in vacuum at 40 °C overnight to give dark blue powders.

Characterization

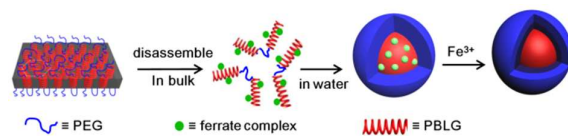
UV-vis spectroscopy data were obtained by use of a Hitachi U3500 at room temperature. FT-IR spectra were recorded using a Nicolet/Nexus 670 FT-IR spectrophotometer. Powder samples were mixed with KBr and then pressed into pellets for FT-IR measurements. Circular dichroism (CD) measurements were recorded on a Jasco J-720 spectropolarimeter in 1 mm quartz cuvettes with a step resolution of 0.2 nm, a scan speed of 50 nm/min, a sensitivity of 0.1 °, and a response time of 9.5 s. Each spectrum was the average of three scans. Dynamic light scattering (DLS) measurement was performed using a Brookhaven instrument. Scattering angle was fixed at 90 °. A field emission gun TEM microscope (JEM2010HR) equipped with an Oxford instrument UTW ISIS EDX system was used to characterize the microstructure of BEB-PB. Acceleration voltage was 200 kV. BEB-PB was dispersed in distilled water with the assistance of sonication (0.05 mg/mL). The sample was prepared by adding a drop of BEB-PB/water suspension on a carbon-coated copper grid. The specimen was directly observed without staining due to the presence of iron elements. X-ray Diffraction (XRD) measurements were performed using XRD diffractometer (D-MAX 2200 VPC) equipped with Ni-filtered Cu K α radiation, having a wavelength of 0.154 nm. The diffractometer was scanned in 2θ range of 1.5°–50° and the scanning rate used was 1.2° min⁻¹. Cyclic voltammetry was performed by using a CHI-660D electrochemical analyzer (CH instruments, Inc.) in a three electrode cell. Glassy carbon working electrodes with a diameter of 3 mm were polished with slurry of 0.05 μ m alumina particles, sonicated and rinsed with ultrapure water. After drying under N₂ flow, the glassy carbon working electrodes were made hydrophilic by the treatment in oxygen plasma (1 Torr O₂, 10 W) for 5 min. The cleaning process was repeated until no voltammetric features were observed between –0.2 and 0.6 V (vs Ag/AgCl) at the scan rate of 100 mV/s in 20 mM sodium phosphate buffer solution. BEB-PB particles dispersed in ultrapure water was deposited on freshly cleaned glassy carbon working electrodes. The solvent was allowed to evaporate at room temperature overnight. To remove oxygen, the 20 mM sodium phosphate buffer solution was degassed by bubbling N₂ for 40 min prior to CV measurements. Every sample was tested three times to obtain reproducible results.

Acknowledgements

The financial support is from NSFC (21074151 and 21374136).

Notes and references

- ^aDSAP lab, PCFM lab, GDHPPC lab, School of Chemistry and Chemical Engineering, Sun Yat-Sen University, Guangzhou 510275, China; E-mail: lgdong@mail.sysu.edu.cn
- ^bInstitute of Textiles & Clothing, The Hong Kong Polytechnic University, Hong Kong, China; E-mail: tcfeib@polyu.edu.hk
- †Electronic Supplementary Information (ESI) available: Calculation of aggregation number of BEB-PB nanoparticles, electrical performance of bare electrodes and conventional PB particles. See DOI: 10.1039/b000000x/
- 1 T. N. Hoheisel, K. Hur and U. B. Wiesner, *Prog. Polym. Sci.*, 2015, **40**, 3–32.
 - 2 J. Kao, K. Thorkelsson, P. Bai, B. J. Rancatore and T. Xu, *Chem. Soc. Rev.*, 2013, **42**, 2654–2678.
 - 3 S. Srivastava, J. L. Schaefer, Z. C. Yang, Z. Y. Tu and L. A. Archer, *Adv. Mater.*, 2014, **26**, 201–233.
 - 4 W. A. Zhang and A. H. E. Muller, *Prog. Polym. Sci.*, 2013, **38**, 1121–1162.
 - 5 N. Yu, X. L. Zheng, Q. Xu and L. H. He, *Macromolecules*, 2011, **44**, 3958–3965.
 - 6 Y. Yu, H. Wen, J. Y. Ma, S. Lykkemark, H. Xu and J. H. Qin, *Adv. Mater.*, 2014, **26**, 2494–2499.
 - 7 C. Stegelmeier, A. Exner, S. Hauschild, V. Filiz, J. Perlich, S. V. Roth, V. Abetz and S. Forster, *Macromolecules*, 2015, **48**, 1524–1530.
 - 8 T. Gegenhuber, A. H. Groschel, T. I. Lobling, M. Drechsler, S. Ehlert, S. Forster and H. Schmalz, *Macromolecules*, 2015, **48**, 1767–1776.
 - 9 J. W. Zhou, G. R. Whittell and I. Manners, *Macromolecules*, 2014, **47**, 3529–3543.
 - 10 Z. K. Zhang, R. J. Ma and L. Q. Shi, *Acc. Chem. Res.*, 2014, **47**, 1426–1437.
 - 11 X. B. Wang, L. Wang, S. X. Yang, M. M. Zhang, Q. Q. Xiong, H. Y. Zhao and L. Liu, *Macromolecules*, 2014, **47**, 1999–2009.
 - 12 J. Huang, R. Y. Wang, Z. Z. Tong, J. T. Xu and Z. Q. Fan, *Macromolecules*, 2014, **47**, 8359–8367.
 - 13 W. N. He, B. Zhou, J. T. Xu, B. Y. Du and Z. Q. Fan, *Macromolecules*, 2012, **45**, 9768–9778.
 - 14 L. Jia, G. Y. Zhao, W. Q. Shi, N. Coombs, I. Gourevich, G. C. Walker, G. Guerin, I. Manners and M. A. Winnik, *Nat. Commun.*, 2014, **5**, 3882.
 - 15 V. Dordovic, M. Uchman, K. Prochazka, A. Zhigunov, J. Plestil, A. Nykanen, J. Ruokolainen and P. Matejcek, *Macromolecules*, 2013, **46**, 6881–6890.
 - 16 J. Y. Zhang, Y. Yan, M. W. Chance, J. H. Chen, J. Hayat, S. G. Ma and C. B. Tang, *Angew. Chem. Int. Ed.*, 2013, **52**, 13387–13391.
 - 17 Y. Yan, J. Y. Zhang, Y. L. Qiao, M. Ganewatta and C. B. Tang, *Macromolecules*, 2013, **46**, 8816–8823.
 - 18 H. Zhou, Y. J. Lu, H. B. Qiu, G. Guerin, I. Manners and M. A. Winnik, *Macromolecules*, 2015, **48**, 2254–2262.
 - 19 X. Roy, J. K. H. Hui, M. Rabnawaz, G. J. Liu and M. J. MacLachlan, *J. Am. Chem. Soc.*, 2011, **133**, 8420–8423.
 - 20 X. Roy, J. K. H. Hui, M. Rabnawaz, G. J. Liu and M. J. MacLachlan, *Angew. Chem. Int. Ed.*, 2011, **50**, 1597–1602.
 - 21 G. D. Liang, J. T. Xu and X. S. Wang, *J. Am. Chem. Soc.*, 2009, **131**, 5378–5379.
 - 22 Y. B. Liu and X. S. Wang, *Polym. Chem.*, 2012, **3**, 2632–2639.
 - 23 S. J. Ye, Y. B. Liu, S. J. Chen, S. Liang, R. McHale, N. Ghasdian, Y. Lu and X. S. Wang, *Chem. Commun.*, 2011, **47**, 6831–6833.
 - 24 R. McHale, N. Ghasdian, Y. B. Liu, M. B. Ward, N. S. Hondow, H. H. Wang, Y. Q. Miao, R. Brydson and X. S. Wang, *Chem. Commun.*, 2010, **46**, 4574–4576.
 - 25 R. McHale, N. Ghasdian, Y. B. Liu, H. H. Wang, Y. Q. Miao and X. S. Wang, *Macromol. Rapid Commun.*, 2010, **31**, 856–860.
 - 26 R. McHale, N. Ghasdian, N. S. Hondow, P. M. Richardson, A. M. Voice, R. Brydson and X. S. Wang, *Macromolecules*, 2010, **43**, 6343–6347.
 - 27 X. X. Ke, J. T. Xu, B. Y. Du and Z. Q. Fan, *Chin. J. Polym. Sci.*, 2015, **33**, 1038–1047.
 - 28 G. D. Liang, H. Ni, S. P. Bao, F. M. Zhu, H. Y. Gao, Q. Wu and B. Z. Tang, *Langmuir*, 2014, **30**, 6294–6301.
 - 29 G. D. Liang, H. Ni, S. P. Bao, F. M. Zhu, H. Y. Gao and Q. Wu, *J. Phys. Chem. B*, 2014, **118**, 6339–6345.
 - 30 L. Yao, Y. Lin and J. J. Watkins, *Macromolecules*, 2014, **47**, 1844–1849.
 - 31 Q. S. Wei, Y. Lin, E. R. Anderson, A. L. Briseno, S. P. Gido and J. J. Watkins, *ACS Nano*, 2012, **6**, 1188–1194.
 - 32 M. P. Kim, D. J. Kang, D. W. Jung, A. G. Kannan, K. H. Kim, K. H. Ku, S. G. Jang, W. S. Chae, G. R. Yi and B. J. Kim, *ACS Nano*, 2012, **6**, 2750–2757.
 - 33 J. M. Hu, T. Wu, G. Y. Zhang and S. Y. Liu, *J. Am. Chem. Soc.*, 2012, **134**, 7624–7627.
 - 34 Y. J. Liu, Y. C. Li, J. He, K. J. Duelle, Z. Y. Lu and Z. H. Nie, *J. Am. Chem. Soc.*, 2014, **136**, 2602–2610.
 - 35 J. He, X. L. Huang, Y. C. Li, Y. J. Liu, T. Babu, M. A. Aronova, S. J. Wang, Z. Y. Lu, X. Y. Chen and Z. H. Nie, *J. Am. Chem. Soc.*, 2013, **135**, 7974–7984.
 - 36 L. Wang, S. J. Zhu, H. Y. Wang, S. N. Qu, Y. L. Zhang, J. H. Zhang, Q. D. Chen, H. L. Xu, W. Han, B. Yang and H. B. Sun, *ACS Nano*, 2014, **8**, 2541–2547.
 - 37 C. X. Wang, Y. Wang, L. Xu, X. D. Shi, X. W. Li, X. W. Xu, H. C. Sun, B. Yang and Q. Lin, *Small*, 2013, **9**, 413–420.
 - 38 M. Gulde, S. Schweda, G. Storeck, M. Maiti, H. K. Yu, A. M. Wodtke, S. Schafer and C. Ropers, *Science*, 2014, **345**, 200–204.
 - 39 M. Tress, E. U. Mapesa, W. Kossack, W. K. Kipnusu, M. Reiche and F. Kremer, *Science*, 2013, **341**, 1371–1374.
 - 40 T. Fukino, H. Joo, Y. Hisada, M. Obana, H. Yamagishi, T. Hikima, M. Takata, N. Fujita and T. Aida, *Science*, 2014, **344**, 499–504.
 - 41 R. H. Deng, F. X. Liang, P. Zhou, C. L. Zhang, X. Z. Qu, Q. Wang, J. L. Li, J. T. Zhu and Z. Z. Yang, *Adv. Mater.*, 2014, **26**, 4469–4472.
 - 42 S. P. Bao, H. Ni, Q. H. Wu, H. Y. Gao, G. D. Liang, F. M. Zhu and Q. Wu, *Polymer*, 2014, **55**, 2205–2212.
 - 43 G. D. Liang, Q. H. Wu, W. P. Qin, S. P. Bao, F. M. Zhu and Q. Wu, *Polym. Chem.*, 2013, **4**, 3821–3828.
 - 44 G. D. Liang, Q. H. Wu, S. P. Bao, F. M. Zhu and Q. Wu, *Polym. Chem.*, 2013, **4**, 5671–5678.
 - 45 F. Armand, H. Sakuragi and K. Tokumaru, *New J. Chem.*, 1993, **17**, 351–356.
 - 46 S. H. Toma, J. A. Bonacin, K. Araki and H. E. Toma, *Eur. J. Inorg. Chem.*, 2007, 3356–3364.
 - 47 S. F. A. Kettle, E. Diana, E. Boccaleri and P. L. Stanghellini, *Inorg. Chem.*, 2007, **46**, 2409–2416.
 - 48 S. Z. Zhan, D. Guo, X. Y. Zhang, C. X. Du, Y. Zhu and R. N. Yang, *Inorg. Chim. Acta*, 2000, **298**, 57–62.
 - 49 P. Papadopoulos, G. Floudas, H. A. Klok, I. Schnell and T. Pakula, *Biomacromolecules*, 2004, **5**, 81–91.
 - 50 G. Holzwarth and P. Doty, *J. Am. Chem. Soc.*, 1965, **87**, 218–228.
 - 51 D. Voet and J. G. Voet, *Biochemistry*, Hoboken, NJ: Wiley, 2004.
 - 52 A. A. Karyakin, *Electroanalysis*, 2001, **13**, 813–819.
 - 53 J. Li, J. D. Qiu, J. J. Xu, H. Y. Chen and X. H. Xia, *Adv. Funct. Mater.*, 2007, **17**, 1574–1580.
 - 54 E. Nossol and A. J. G. Zarbin, *Adv. Funct. Mater.*, 2009, **19**, 3980–3986.
 - 55 W. Chen, S. Cai, Q. Q. Ren, W. Wen and Y. D. Zhao, *Analyst*, 2012, **137**, 49–58.
 - 56 A. A. Karyakin, E. E. Karyakina and L. Gorton, *Electrochem. Commun.*, 1999, **1**, 78–82.



A conceptually new approach for synthesis of tiny hybrid nanoparticles through direct disassembly-assisted synthesis (DDAS) strategy has been developed.